SSRG International Journal of Geo-informatics and Geological Science
ISSN: 2393–9206 / https://doi.org/10.14445/23939206/IJGGS-V10I2P103

Volume 10 Issue 2, 18-25, May-Aug 2023

Original Article

Improved Fault and Reservoir Channel Delineation of a Gas Field in the Onshore Niger Delta Basin

Inichinbia Sonny[1], Adizua Okechukwu Frank[2]

[1,2]*Geophysics Research Group – GRG, Department of Physics, Faculty of Science, University of Port Harcourt, Port Harcourt, Rivers State, Nigeria.*

[2]*Corresponding Author : okechukwu.adizua@uniport.edu.ng*

Received: 15 June 2023 Revised: 28 July 2023 Accepted: 12 August 2023 Published: 31 August 2023

Abstract *- A discovered and unitized gas field of the Nigerian Delta, through an initial 2D seismic survey and drilled well, is being studied. Imaging of the crest of the structure remained very poor. Uncertainties about the lateral extent of the reservoirs, pinchout, distribution of reservoir properties, and fault positions along the reservoirs were some challenges that were not yet fully understood in the study area. Hence, some of the risks associated with the field were fault and seal integrity, sand development, overpressures and reservoir rock properties. There were also exploration challenges in the data set of the field, such as the discrimination of hydrocarbon-bearing sands from shales and, more importantly, the separation of gas sands from brine-saturated sandstones. In order to address these issues, new 3D prestack seismic data were acquired with long offset cable and high fold of coverage, giving better resolution and structural interpretation across the reservoirs of interest. The current challenge was, therefore, to use the newly processed anisotropic 3D prestack seismic data to de-risk the reservoirs' variability and heterogeneity and select locations for new development wells. Full, near, mid and far sub-stacks were generated to aid structural interpretation. Using anisotropic 3D seismic reflection data calibrated to well data, closely spaced, low displacement, planar, normal growth faults were mapped within the Tertiary Agbada Formation. A series of seismic horizontal time slices and computed seismic attributes were used to interpret the configuration of these faults. The closely spaced faults display an east-west trend. Accurate interpretation of the faults has enabled precise location of the faults and their orientation, style, and density, intending to reduce drilling risks and hazards.*

Keywords *- 2D seismic survey, 3D prestack seismic data, Fault and seal integrity, Drilling risks and hazards, De-risking and new development wells.*

1. Introduction

Through seismic interpretation, seismic data is used to create and interpret geologically plausible models and explain discontinuities, traps, and seals such as faults on 3D seismic volumes. It also enables us to understand the trapped infill fluid(s), map facies and reduce hazards/risks. Fault zones are typically associated with different types of seismic characters, such as reflection terminations, dip changes of seismic reflectors, seismic waveform changes, loss in signal energy, frequency content, etc. However, in seismic sections, geophysicists often represent faults as amplitude discontinuities and fault interpretation plays a key role in subsurface structural characterization for hydrocarbon exploration and development, planning, and placement of wells. It is worthy of note that the complexity of geologic structures, the presence of noise, diffraction and dispersion effects, etc, in the seismic data masks coherent images and hampers clear detection of faults. This makes fault interpretation a complex task requiring significant effort and time, leading to several actions being taken to resolve these challenges. Some of the efforts include deploying several sophisticated algorithms that measure lateral similarities between seismic traces or reflector geometries and improved dip computational skills. Also, novel techniques have evolved, using geometric and structural attributes that identify and enhance amplitude discontinuities. Furthermore, novel methods that improve the lineaments detected earlier by the geometric/structural attributes and optimized fault detection and enhancement are incorporated. With these advances, fault interpretation has essentially improved subsurface characterization for the precise location of faults and their orientation, style, density, etc., which is important in reducing drilling risks and hazards [1-4].

This research work acquired a new 3D seismic dataset over the field. The new 3D seismic was expected to significantly improve the data quality in the crestal area through improved illumination in terms of hits per bin and more uniform illumination. In addition to the new 3D seismic, a pre-drilled development well and potential well

test were used to assess the productivity and compartmentalization level and guide the placement and number of subsequent development wells. The Nigerian Delta is controlled and characterized by an extensive regime where various arrangements and structural elements have been documented in the Basin. The study is focused on the location, style, orientation and density of faults in the field.

2. Location and Geology of the Study Area

The field lies within the Niger Delta Basin and measures about 12 km by 5 km. It is still a prospect and has not yet been fully appraised. The Niger Delta lies between latitudes 4° N and 6° N and longitudes 3° E and 9° E. The Niger Delta Basin is a coarsening upward regressive sequence of Tertiary clastic sediments divided into three lithostratigraphic units representing prograding depositional facies. These units are distinguished mostly based on sand/shale ratios as follows: firstly, the Akata Formation is at the base of the delta; secondly, the Agbada Formation overlies the Akata Formation; and thirdly, Benin Formation is the topmost, overlying the Agbada Formation. Knowledge and understanding of the geology of the Niger Delta were obtained from the detailed works of [5-13].

The structure of the field is an elongated rollover anticline bounded to the south and southeast by large boundary faults that throw down towards the south and southeast. Towards the north is a regional growth fault that joins with the northeastern boundary fault to close the structure towards the east. It is a fault-dip closure against a large growth fault which separates it from a neighboring southern field. H4000 hydrocarbons are trapped in a closure against the southern and southeastern faults.

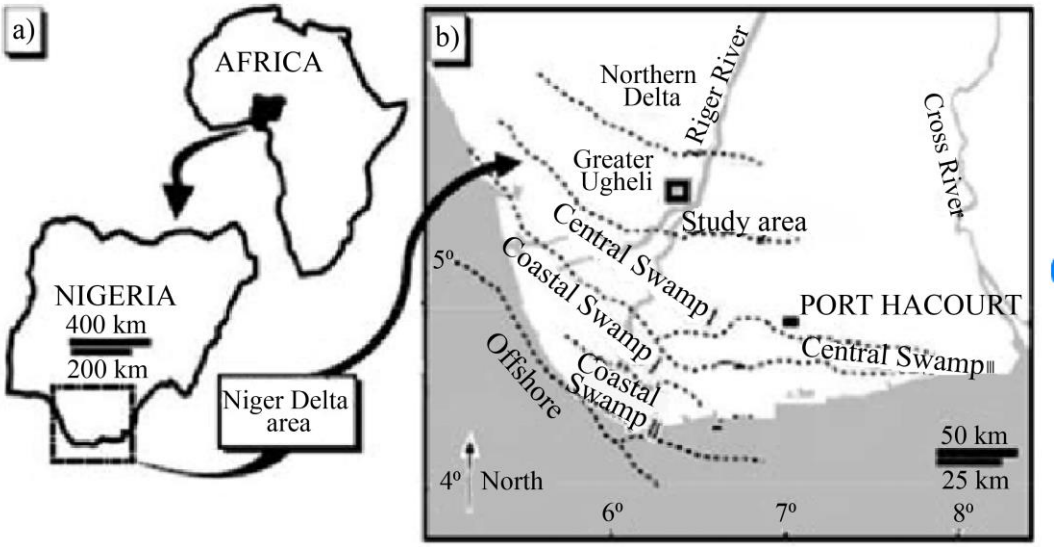

Fig. 1 Map of the Niger Delta Basin showing the approximate location of the study area (Adapted from [6])

3. Materials and Methods

An initial 2D and a recent 3D seismic survey covered the field. A high-quality anisotropic 3D depth migrated seismic volume covering an approximate area of 60.0 km^2 consisting of inline and crossline spacing of 25.0 m with a sample rate of 4.0 ms was analyzed. In-depth, the seismic volume has a record length of 5.80 s two-way travel time with an average frequency content of 42.0 Hz. Seismic data is reasonably good down to 2.5 s, below which deeper events were poorly defined and discontinuous. A velocity checkshot was taken in well 001, well 004 and well 005. The field consists of a stacked sequence of reservoirs in shore-face and channel deposits.

In an effort to improve the image at the crest in the fault shadow zone, the data was reprocessed with industry-proprietary PreSDM workflows. Full, near, mid and far sub-stacks were generated to aid well-to-seismic tie and structural interpretation [2, 3, 15]. The method was robust, attenuating seismic noise and unmasked amplitude discontinuities to illuminate geologic structures properly. This provided clear fault volumes and accurate imaging of the subsurface that enhanced interpretation. All the datasets have the SEG-Y normal polarity convention.

4. Results and Interpretation

The execution of the new 3D seismic survey aimed to improve the quality of the existing 2D seismic dataset, particularly in crestal areas, to support future drilling development. The new dataset was an improvement that significantly reduced structural uncertainty over the flank area, yet imaging in the crestal area remained sub-optimal. This new seismic volume (Figure 2) will be deployed for the well location optimization and depth prognosis in the well

proposals. Figure 2 shows how amplitude discontinuities have been improved, and logs from the wells overlay the seismic section; faults and horizons were also highlighted. Several unconformities were seen in the seismic data. The Tertiary age siliciclastic deposits forming the Niger Delta were attributed to three different lithostratigraphic formations – the Akata Formation, the Agbada Formation, and the Benin Formation. The Agbada Formation (Paralic Cycles) makes up the majority of the oil and gas reservoirs of the Niger Delta Basin, including the study area. It comprises alternating sandstone/shale bed sets interpreted to represent the delta front, distributary channels and the deltaic plain. The upper part has higher sandstone content than the lower part, demonstrating the progressive seaward advance of the Niger delta through geological time [5-13]. The structure was bound to the south and the southwest by large faults that throw down towards the south/southeast. Towards the north is a regional growth fault that joins the northeastern boundary fault to close the structure towards the east. The western (aquifer) part of the structure is not covered by the 3D seismic data, but the fact that the reservoirs are over-pressured suggests another bounding fault there. It is bounded north and south by large listric normal faults associated with gravity collapse in the delta [6-13].

The hydrocarbon-bearing intervals of the field form part of a succession of Tertiary proximal deltaic deposits separated by laterally extensive shales and shaly heterolithic packages that represent flooding episodes. The sand packages were progradational units that progressed upwards from medium-quality shore-face into good-quality channel units. Laterally extensive channel cuts were filled by a combination of coarse braided fluvial sands, localized delta top shales, and finer shore-face deposits interlayered with thin marine shales.

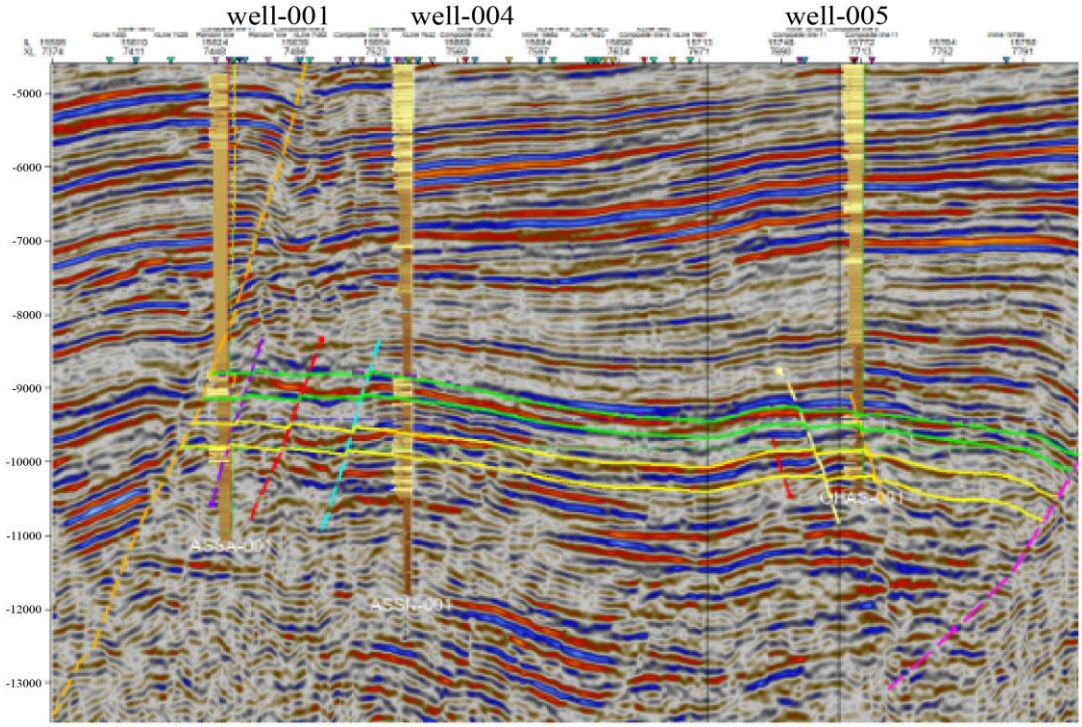

Fig. 2 Seismic cross section showing H1000 and H4000 sands in well-001, well-004 and well-005. The lineaments show less seismic noise, and faults were easily detected

The depositional direction was interpreted to be from north to south [5-7, 12,13].

Fault interpretation has been refined on the new dataset to a final increment of 400 m, directionally dependent on fault orientation, and included all faults visible in the interval from the shallow to the deeper reservoirs. Where necessary, for resolving geometry complexity, the picking grid was refined to 200 m or every 8th line (e.g. H1000 and H4000 tops around well-004 and well-005), shown in Figure 3. In addition, merged 3D DMO data from a neighboring field was used to structurally constrain the northern and northeastern parts of the boundary faults. The current intra-field fault interpretation was guided by inspecting vertical reflectivity display and semblance attribute maps generated from the PreSDM dataset. The definition of the faults was based on the inspection of vertical reflectivity displays and semblance data in the horizon and time slices, as shown in Figures 3, 4, 5 and 6. The structural framework was similar for the H1000 and the H4000.

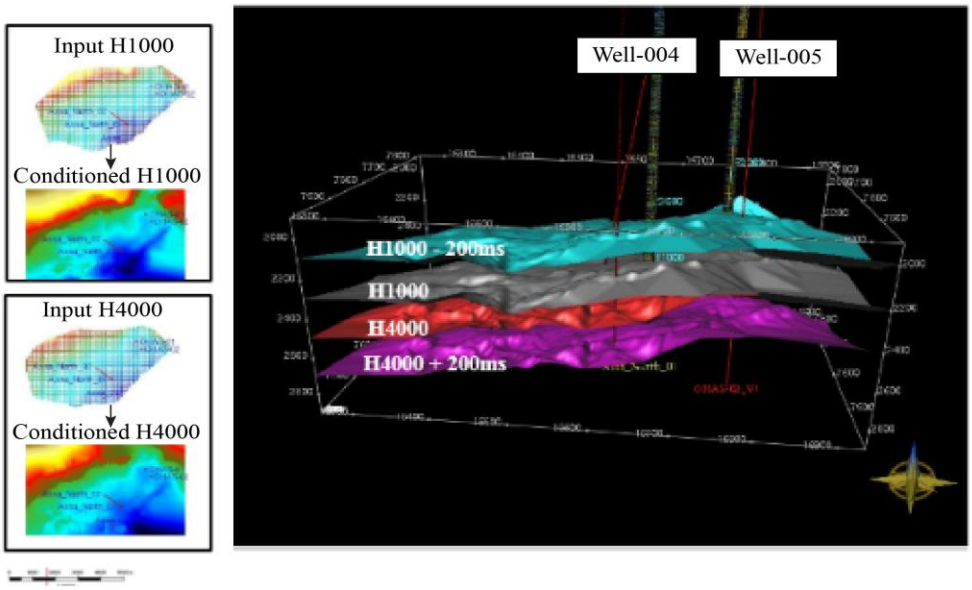

Fig. 3 Refined picking grid and interpreted horizons with well-004 and well-005 [16]

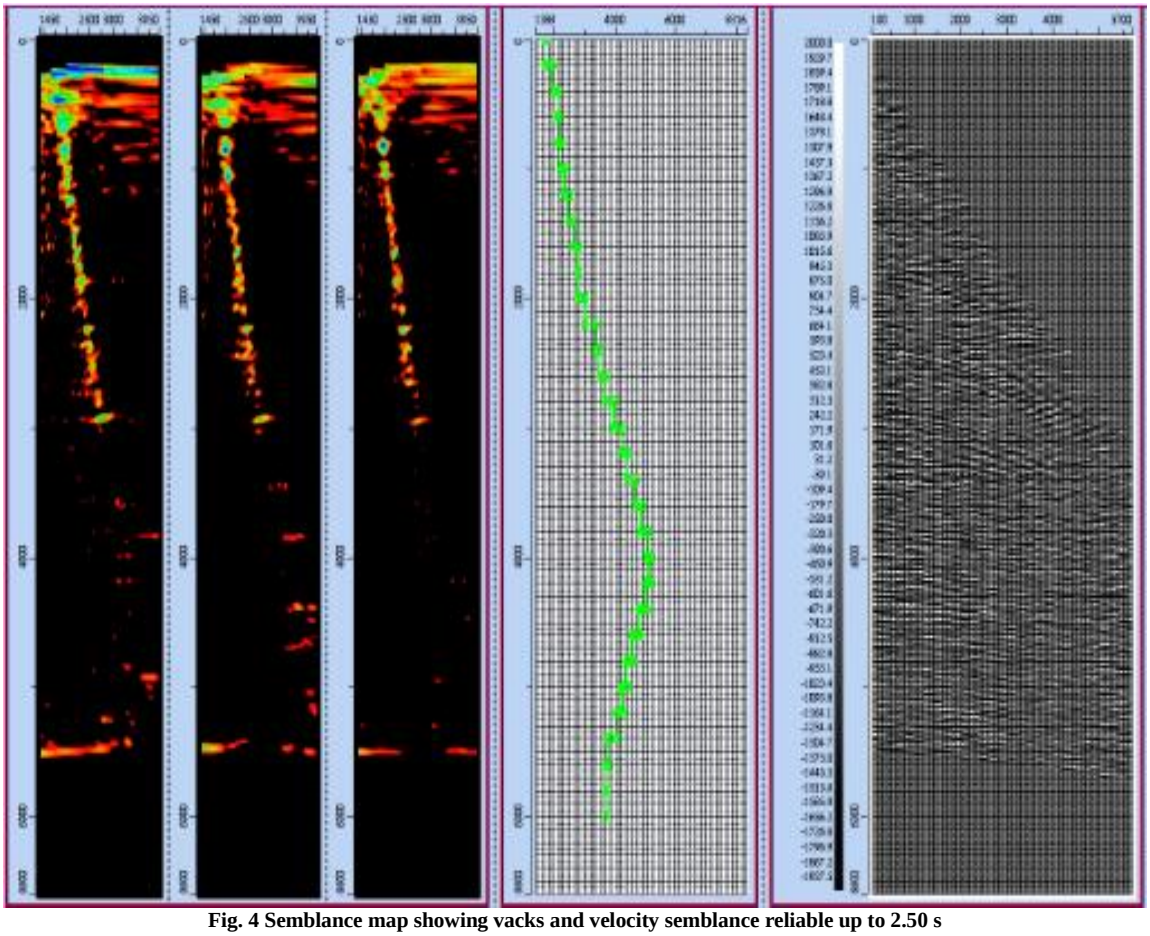

Fig. 4 Semblance map showing vacks and velocity semblance reliable up to 2.50 s

The seismic interpretation and static/dynamic modeling generated two principal faulted zones, one adjacent to the southeastern (SE) boundary fault and the other located against the southern boundary (bounding) fault (where well-003 was drilled). Further analysis indicated faults not extensive (about 2-3 km) and largely parallel to the SE boundary fault.

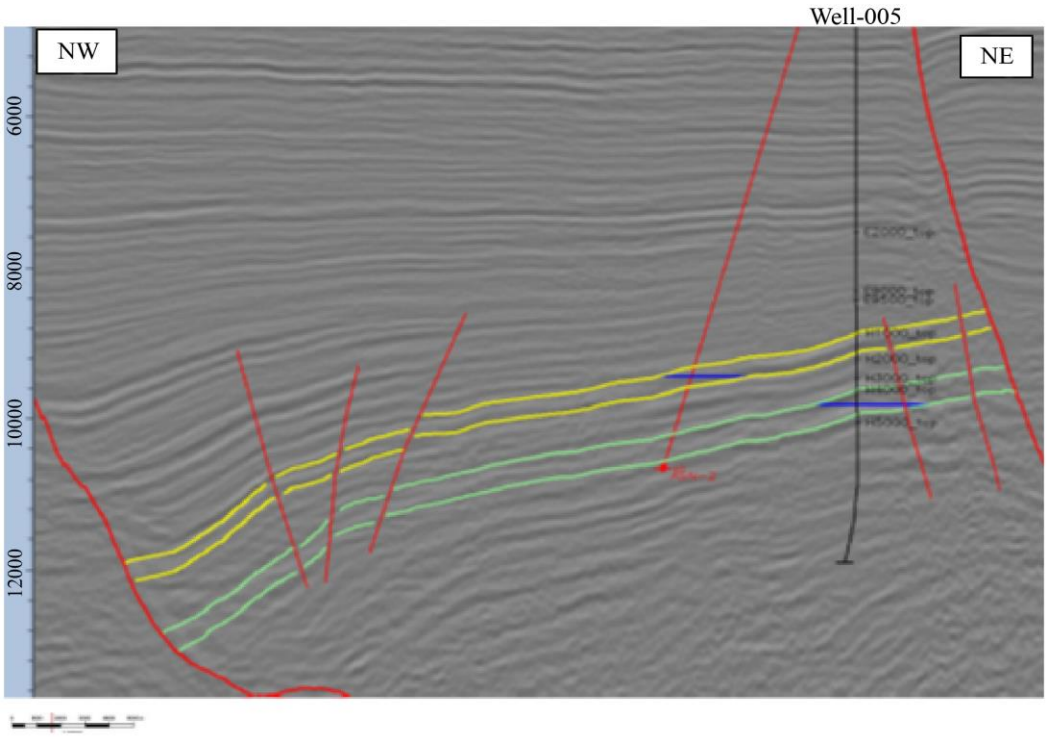

Fig. 5 Band-limited seismic data showing seismic events smoothed out and random noise attenuated. Discontinuities are unmasked and clearer

Figure 6 displays the sliced time/depth structure maps and modeled faults for the H1000 and H4000 reservoirs. The structure is bound to the south and the southwest by large faults that throw down towards the south/southeast. A regional growth fault joins the northeastern boundary fault towards the north to close the structure towards the east. The fact that the reservoirs are over-pressured suggests another bounding fault may be present. At the H1000 level, the field measures some 12 km long and 5 km wide. The crest is in the southeastern corner at approximately 8,500 ft, and the hydrocarbon-water contact at 9,435 ft TVDss yields a column of some 950 ft. The preferred interpretation for the difference in fluid type and hydrocarbon-water contact between well-004 and well-001 at the H4000 level is that sealing is the small fault that separates them. The preferred interpretation of the well-001 test at the H4000 level suggests the presence of a sealing barrier some 0.5 km from where the main boundary fault is mapped on the seismic section.

The existence of compartments in the H1000 and H4000 crestal areas is based on the interpretation of the well-001 well test. The H4000 well-test interpretation described an event that can be interpreted as either a fluid contact or a sealing fault. The current seismic section does not indicate faults large enough to completely offset either the H1000 or H4000 reservoirs. A fault has been modeled as a link-up of a number of potential smaller faults. Fault seal analysis showed that the risk of this fault holding a large H1000 or H4000 column, rendering the crestal area water-bearing, is highly unlikely. But there is a possibility that the crestal area may be more faulted than currently modeled and that the proposed well count and location cannot effectively access the gas and condensate. The consequence of more compartmentalization would be additional development wells and the requirement of a second drilling location.

Well-002 reduces the uncertainty regarding the crestal area volumes in the H1000 reservoir. The northeastern fault is sealing at the H4000 level (different fluid contacts in well-001 and well-004) but not at the H1000 level (similar fluid contacts). The probability that the Southern block fault is sealing and holding a large H1000 column is extremely low, and it is considered not very likely that the crestal area is water-bearing. The time structure maps show a complex structural configuration with the presence of several highs and lows. The existence of compartments in the H1000 and H4000 crestal areas is based on the interpretation of the well-002 well test. One of the faults is sealing at the H4000 level (different fluid contacts in well-002 and well-004) but not at the H1000 level. H1000 hydrocarbons are trapped in a closure against the southern and southeastern faults. The crest is in the southeastern corner at approximately 2,590.80 m (8,500 ft). The H1000 reservoir dips towards the northwest, with a dip of some 3.5º across the hydrocarbon-filled area and steeper in the aquifer.

Figure 7 shows the detailed delineation of the structure as currently improved by better imaging in the crestal areas at the southeastern and southern edges of the field, in the shadow zone of the large boundary faults.

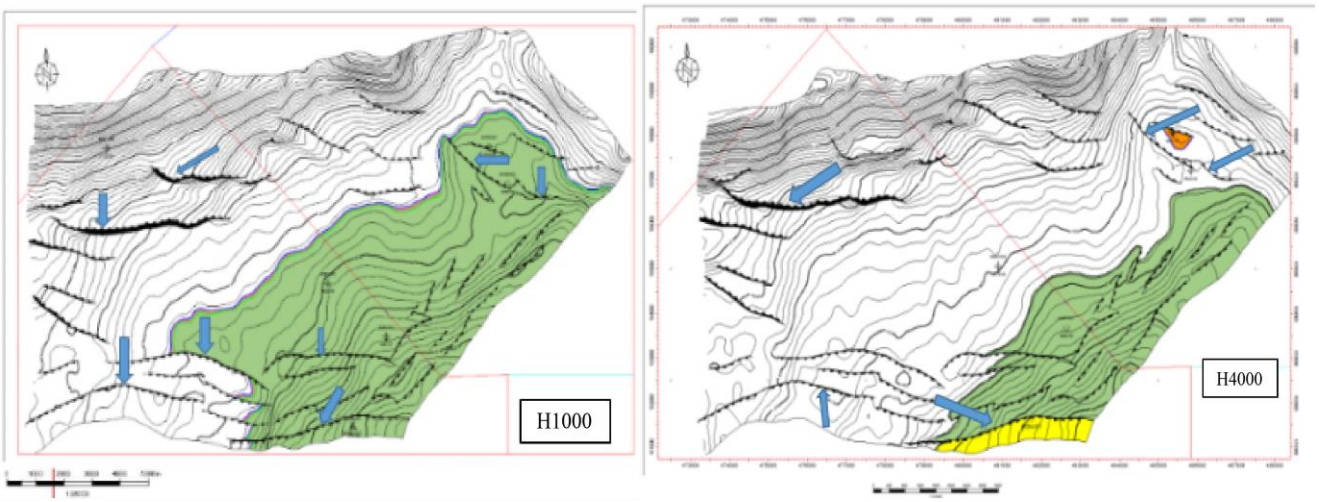

Fig. 6 Time/depth structure contour maps of tops of the H1000 and H4000 reservoirs showing the modeled faults and drilled wells in the study area. The locations of seismic lines (in red) across the structure are indicated

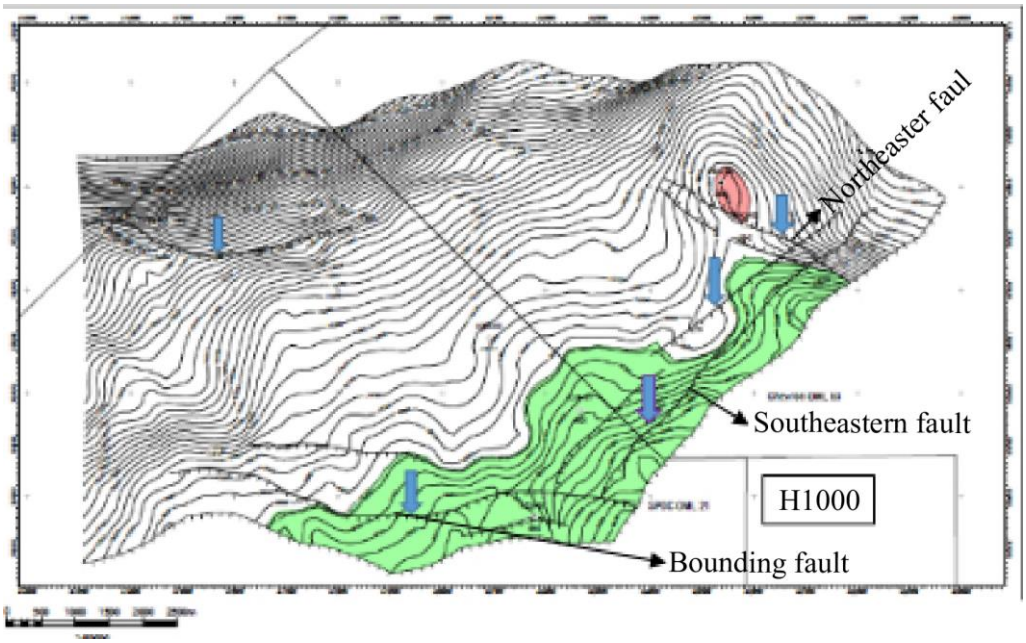

Fig. 7 The H1000 top sliced depth map and modeled faults as interpreted from the 3D seismic data. The contour interval is 50 m. The shaded areas (in green) are proven hydrocarbon-saturated areas. The structure also shows some major faults and drilled wells in the study area (Courtesy: SPDC, Nigeria Ltd.)

H4000 closure resides in the footwall side of the southern and southeastern boundary faults. Three wells penetrated H4000; however, gas was detected by well-002 only. Well-006 is water-bearing, and well-004 has an oil-water contact. The number of faults is enormous with well-defined trending. The structure is an elongated rollover anticline bounded to the south and southwest by large boundary faults that throw down toward the south and southeast. A regional growth fault toward the north joins the northeastern boundary fault to close the structure toward the east. It is a fault deep closure against a large growth fault, which separates it from a neighbouring field. Three H4000 structural realizations were built from the base case, minimum and maximum top structure maps and two isochrons. H4000 sands were interpreted to represent a series of channelized shoreface deposits (where channels are fluvial-dominated). Furthermore, a thick channel is interpreted as a tidal channel at well-002 but as a more fluvial-dominated channel in well-005 (to the east) and at well-006 (to the west).

The main factors contributing to structural uncertainty are picking uncertainty (in particular at the fault shadow zones), areas of intense synthetic and antithetic faulting and velocity uncertainty. There is a smaller scale, intra-block faulting parallel to the southeastern and southern major

boundary fault that may either create pathways for the gas from the various sub-units to connect or, if sealed, cause compartmentalization. Well, tests taken at well-001 have detected a boundary effect that can be attributed to faults of this type.

5. Discussion

The distance between well-001 and well-004/well-005 is 5 km. The field's sediments comprise a series of sand and shale successions deposited during different relative sea level changes. These sediments have characteristic coarsening-upward, fining-upward, and blocky and serrated gamma ray and self-potential log profiles. The sands were deposited within a thick shale package and are dominated by incised prograding shore-face deposits. The H1000 and H4000 sands are thicker sands comprised of more stacked channel sand deposits with some estuarine influences and tidal channel deposits. Within the field, the sands were laterally continuous with a slight thickening to the north due to syn-sedimentary activity on the growth fault just north of the well-006. The H1000 and H4000 sands have been correlated at higher resolution using sequence stratigraphic interpretations between the six wells in the field area [16].

Sands and shales thicken to the north (well-003 to well-006) due to syn-sedimentary activity on the growth fault north of the field. Sediment influx was from the north of the field. Well-001 encountered a gas down to (GDT) in the H1000 reservoir and a Gas-Water-Contact (GWC) in the H4000 and yielded high-quality pressure data across a wide depth range, and Pressure, Volume, Temperature (PVT) samples from both H1000 and H4000. Both reservoirs were found to be over-pressured by some 2000 psi (~ 0.66 psi/ft). The shallower reservoirs overlying the H1000 reservoir were separated by a regional shale package several thousand feet thick that hampers effective dewatering of the underlying sediments and controls the onset of overpressures. The shallower reservoir sands are hydrostatically pressured, while the underlying H1000 and H4000 reservoirs are over-pressured by some 2000 psi. At the crest of the field, well-003 targeting shallower reservoirs in the hanging wall of the bounding fault intersect the bounding fault and penetrate the northwest block. It also encountered a GDT in the H1000, while the H4000 was faulted out.

Generally, the sediments represent fluvio-deltaic deposits, recording a series of relative sea-level falls followed by flooding. The H1000 sands contain four system tracts dominated by amalgamated channel packages. Little or no shore-face remains in the upper tracts where channels have eroded into the underlying shale units. There are three internal correlatable flooding surfaces separating four para-sequences characterized by an alteration of shale and thick sand packages. The para-sequences are split into shale and sand units, correlatable field-wide. The log profile is blocky and fining upward, with a more variable but overall coarsening-up log character [16].

The H4000 sands contain four system tracts where shore-face to-channel progradations are preserved. Six main genetic facies are identified: marine shale, lower shore-face, upper shore-face, tidal channel, channel and channel heterolithics. Three internal correlatable flooding surfaces are separating four para-sequences. The character of each para-sequence varies from well to well, and facies correlation is more complicated than in the H1000 reservoir. Overall, the shore-face packages are preserved better than in the H1000, but they do not exist at every well for every reservoir unit. Each para-sequence generally displays shale, overlain by a coarsening-up profile that passes upwards into a blocky, fining-upward profile. The coarsening-upward successions are interpreted to represent shore-face deposits, while the blocky to fining-upward successions are interpreted to represent channel deposits. The blocky log character sand units are interpreted to represent thick amalgamated channel sands. The general absence of shore-face units at their base is due to erosion by these channel packages. This is supported by the thickness of the channel packages. The more variable log character sand units were interpreted to represent shore-face sands. The H4000 sands were interpreted to represent a series of channelized shore-face deposits (where channels are fluvial dominated).

From well to well, the amount of shore-face deposits in each para-sequence varies due to the localization of channels, which erode underlying deposits in a non-uniform manner. The quality and type of channel varies from well to well. Most channel sands were thought to be fluvial dominated except in the deeper reservoir of well-001, where the channel is tidally dominated. Here, the channel is very heterogeneous with sand and shale interbeds, but this passes laterally into fluvial-dominated channels well-005 (to the East) and well-002 (to the West). The lithology is dark grey, silty, calcareous and frangible.

6. Conclusion

Fault interpretation has been refined on the new dataset, and fault images have been delineated accurately, reducing seismic noise and artifacts and saving interpretation time and effort. The fault models were accurate and reliable, and the fault planes coincided with the lineaments on the seismic section. The structural trends were in agreement with documented evidences. Seismic interpretation revealed three principal faulted zones: the northeastern fault adjacent to the SE boundary fault and the last located against the southern boundary fault, where well-003 was drilled. The base case interpretation models the southeastern fault and bounding fault as a link-up of a number of potential smaller faults. The probability that the southeastern fault complex is holding back a large H1000 and H4000 column, rendering the crestal area water bearing as was believed earlier, is extremely low,

as the maximum throw mapped is less than 100 ft (compared to the overall thickness of the H1000 and H4000 of 375 and 285 ft respectively) as displayed in Figure 6. Fault seal analysis indicated that for the H1000 crestal fault, the fault transmissibility was about 0.12, while for the H4000 crestal fault, the fault transmissibility was about 0.05.

Acknowledgements

The authors are grateful to Shell Petroleum Development Company (SPDC) of Nigeria Limited for providing the data. Our gratitude also goes to the staff of the various asset teams of the Company for their assistance and invaluable contributions to this work. The authors also wish to express their profound thanks and gratitude to Seventh Sense Research Group – SSRG, India, the publishers of the International Journal of Geoinformatics and Geological Science – IJGGS for graciously approving and granting a full publication fee waiver for this research paper. We are highly indebted to your Organization for promoting and giving our research programs a huge boost.

References

[1] Heather Bedle, and Jean-Paul van Gestel, "Introduction to this Special Section: Seismic Interpretation," *The Leading Edge*, vol. 40, no. 7, pp. 482-483, 2021. [CrossRef] [Google Scholar] [Publisher Link]

[2] Mateo Acuña-Uribe et al., "Enhanced Ant Tracking: Using a Multispectral Seismic Attribute Workflow to Improve 3d Fault Detection," *The Leading Edge*, vol. 40, no. 7, pp. 502-512, 2021. [CrossRef] [Google Scholar] [Publisher Link]

[3] Mike Bahorich, and Steve Farmer, "3D Seismic Discontinuity for Fault and Stratigraphic Features: The Coherence Cube," *The Leading Edge*, vol. 14, no. 10, pp. 1053-1058, 1995. [CrossRef] [Google Scholar] [Publisher Link]

[4] Sheena A D, "Seismic Noise Removal and its Applications - A Review of Exploring Wavelet Transform in Civil Engineering," *SSRG International Journal of Civil Engineering*, vol. 4, no. 12, pp. 1-6, 2017. [CrossRef] [Google Scholar] [Publisher Link]

[5] Michele L. Tuttle, Ronald R. Charpentier, and Michael E. Brownfield, *The Niger Delta Petroleum System, Niger Delta Province, Nigeria, Cameroun and Equatorial Guinea, Africa*, US Geological Survey, United States of America, pp. 6-29, 1999. [CrossRef] [Google Scholar] [Publisher Link]

[6] K. C. Short, and A. J. Stäuble, "Outline of Geology of Niger Delta1," *American Association of Petroleum Geology Bulletin*, vol. 51, no. 5, pp. 761-779, 1967. [CrossRef] [Google Scholar] [Publisher Link]

[7] Harry Doust, and Ebi Omatsola, *Niger Delta*, Divergent/Passive Margin Basins, American Association of Petroleum Geologists Memoir, vol. 48, pp. 201-238, 1989. [CrossRef] [Google Scholar] [Publisher Link]

[8] Uwadiegwu Promise, C.N. Nwankwo and S.U. Eze, "Quantitative Analysis of Seismic Refraction Data to Delineate the Weathering Structures in Parts of Delta State," *SSRG International Journal of Applied Physics*, vol. 5, no. 2, pp. 19-24, 2018. [CrossRef] [Google Scholar] [Publisher Link]

[9] S. Pochat et al., "A Simple Method of Determining Sand/Shale Ratios from Seismic Analysis of Growth Faults: An Example From Upper Oligocene to Lower Miocene Niger Delta Deposits," *The American Association of Petroleum Geologists Bulletin*, vol. 88, no. 10, pp. 1357-1367, 2004. [Google Scholar] [Publisher Link]

[10] R. M. Bustin, "Sedimentology and Characteristics of Dispersed Organic Matter in Tertiary Niger Delta: Origin of Source Rocks in a Deltaic Environment," *The American Association of Petroleum Geologists Bulletin*, vol. 72, no. 3, pp. 277-298, 1988. [CrossRef] [Google Scholar] [Publisher Link]

[11] P. Stacher, "Present Understanding of the Niger Delta Hydrocarbon Habitat," *Pascal and Francis Bibliographic Databases*, pp. 257-267, 1995. [Google Scholar] [Publisher Link]

[12] Devdatta K. Mokashi, and Vidula S. Sohoni, "Identification of Water Conservation Zone by Application of Electrical Resistivity Method in Parts of Osmanabad District, Maharashtra-India," *International Journal of Engineering Trends and Technology*, vol. 69, no. 3, pp. 233-238, 2021. [CrossRef] [Google Scholar] [Publisher Link]

[13] Joseph I. Nwachukwu, and Patricia I. Chukwura, "Organic Matter of Agbada Formation, Niger Delta, Nigeria," *The American Association of Petroleum Geologists Bulletin*, vol. 70, no. 1, pp. 48-55, 1986. [Google Scholar] [Publisher Link]

[14] Muhajir Anshori et al., "Ambient Noise Tomography for Determining the Velocity Model of Rayleigh Wave in Java Island, Indonesia," *SSRG International Journal of Applied Physics*, vol. 5, no. 1, pp. 9-13, 2018. [CrossRef] [Google Scholar] [Publisher Link]

[15] Doha Monier, Azza El Rawy, and Abdullah Mahmoud, "Delineation of Reservoir Channels by Different Seismic Attributes and Geobody Extractions for Robust Volumetric Estimation, Safron Field, Offshore Nile Delta, Egypt," *The Leading Edge*, vol. 40, no. 7, pp. 484-493, 2021. [CrossRef] [Google Scholar] [Publisher Link]

[16] S. Inichinbia, and Halidu Hamza, "Detailed Quantitative Sequence Stratigraphic Interpretation for the Characterization of Amangi Field Using Seismic Data and Well Logs," *Scientia Africana*, vol. 19, no. 3, pp. 63-82, 2020. [CrossRef] [Google Scholar] [Publisher Link]